# Supporting Information

# Voltammetric and spectroscopic characterization of early intermediates in the Co(II)polypyridyl-catalyzed reduction of water

Wangkheimayum Marjit Singh, Mohammad Mirmohades, Reuben T. Jane, Travis A. White, Leif Hammarström, Anders Thapper, Reiner Lomoth* and Sascha Ott*

Department of Chemistry, Ångström Laboratory
Uppsala University
Box 523, 751 20 Uppsala, Sweden
Fax: (+46) 18-471-6844
Email: reiner.lomoth@kemi.uu.se, sascha.ott@kemi.uu.se

**Table of Contents**

## Materials and Syntheses

**Materials:** All chemicals and reagents were used as received unless otherwise noted. N-Bromosuccinimide (NBS) was purified by recrystallization from boiling water, dried *in vacuo*, and stored under argon atmosphere.

**N-methyl-N-(2-pyridinylmethyl)-2,2′-bipyridine-6-methanamine (bpma):** To a solution of 6-(bromomethyl)-2,2'-bipyridine[1] (0.25 g, 1.0 mmol) in acetonitrile (25 ml) was added 1 equivalent of 2-[(methylamino)methyl]pyridine (0.12 g, 1.0 mmol) at RT. *N*,*N*-Diisopropylethylamine (0.26 ml, 1.5 mmol) was added drop-wise to ice cooled condition. The reaction mixture was stirred at RT for 5 h. Upon complete consumption of 6-(bromomethyl)-2,2'-bipyridine, water (50 mL) was added, and the product was extracted into ethyl acetate (3 × 50 mL). The combined organic layers were dried over anhydrous $MgSO_4$, filtered and evaporated under reduced pressure to afford the crude compound. The crude product was dissolved in hexane (50ml) and evaporated under reduced pressure (repeated two times) to give pure product as yellow oil (0.26 g, 89%). $^1$H NMR ($CDCl_3$, 300 MHz): δ 2.41 (s, 3H, -$CH_3$), 3.87 (s, 2H, pyridyl methylene), 3.91 (s, 2H, bipyridyl methylene), 7.18 (t, *J* = 8.0 Hz, 1H), 7.30 (t, *J* = 8.0 Hz, 1H), 7.59 (d, *J* = 12.0 Hz, 2H), 7.69 (d, *J* = 12.0 Hz, 1H), 7.81 (m, 2H), 8.29 (d, *J* = 12.0 Hz, 1H), 8.47 (d, *J* = 12.0 Hz, 1H), 8.58 (d, *J* = 4.0 Hz, 1H), 8.69 (d, *J* = 8.0 Hz, 1H). ESI-MS: m/z $[M + H^+]^+$ = 291.1 (Calcd m/z for bpma = 290.3).

**[Co(bpma)$Cl_2$]:** To a suspension of bpma (0.10 g, 0.36 mmol) in $CH_3CN$ (5 mL), $CoCl_2 \cdot 6H_2O$ (0.086 g, 0.36 mmol) in $CH_3CN$ (3 mL) was added at RT. The resulting solution was stirred for 1 h at RT. The light pink precipitate that formed was filtered through a glass frit membrane, washed with diethyl ether (5 ml × 5), and dried under vacuum to give the desired product (0.11 g, Yield: 73%). Crystals suitable for X-ray diffraction were obtained by diffusion of diethyl ether into a methanol solution of the compound at 4°C. Anal. Calcd for $C_{18}H_{18}Cl_2CoN_4$: C, 51.45; H, 4.32; N, 13.33. Found: C, 51.31; H, 4.25; N, 13.34. ESI-MS: m/z = 385.4 (Calcd m/z for $[M - Cl^-]^+$ = 384.1).

## Instrumentation and Experimental Procedures

HPLC-MS data were obtained using a Dionex UltiMate 3000 system on a Phenomenex Gemini C18 column (150 x 3.0 mm, 5µm) coupled to a Thermo LCQ Deca XP Max with electrospray ionization. Solvents used for HPLC: 0.05% formic acid in $H_2O$ and 0.05% formic acid in $CH_3CN$. $^1$H-NMR spectra were obtained using a Varian 300 MHz spectrometer at 293 K with $CDCl_3$ as the solvent. Chemical shifts are reported in ppm and referenced internally to the residual solvent signal. Elemental analysis (CHN) was performed by Analytische Laboratorien (Germany). Photocatalytic reactions were carried out using a LED-Stab 54 LED array (INNOTAS Elektronik GmbH, Zittau, Germany) with $\lambda$ = 470 nm and photon flux = 4.9 x $10^{20}$ photons/sec. The amount of photocatalytically produced $H_2$ gas in the head space was detected using a HY-OPTIMA Model 740 solid-state $H_2$ sensor ($H_2$scan; Valencia, CA, USA).

**Electrochemistry:** Electrochemical measurements were performed in either $CH_3CN$ solution (distilled over $CaH_2$) containing 0.1 M $Bu_4NPF_6$ as the supporting electrolyte (dried at 80°C *in vacuo*), or a Britton-Robinson aqueous buffered solution (0.04 M $H_3BO_3$, 0.04 M $H_3PO_4$, and 0.04 M $CH_3COOH$ titrated to desired pH using NaOH)[2] at pH values ranging from 5.32-13.76. All experiments were performed at room temperature and all solutions were deoxygenated with solvent-saturated argon prior to use. Cyclic voltammetric measurements (CVs) were performed using a one-compartment, three-electrode configuration connected to an Autolab PGSTAT100 potentiostat controlled with GPES 4.9 software (Eco Chemie). The working electrode was a 3 mm glassy carbon disc that was polished with 0.05µm alumina prior to use. The counter electrode was a glassy carbon rod and the reference electrode was either a non-aqueous $Ag/Ag^+$ electrode (10 mM $AgNO_3$ in $CH_3CN$ for non-aqueous measurements) or an Ag/AgCl electrode (sat. KCl in $H_2O$ for aqueous measurements). Ferrocene was used as an external standard for the non-aqueous measurements and values were converted to versus the $Fc^{+/0}$ couple by the addition of 0.06 V.

**Spectroelectrochemistry:** Electronic absorption spectra were recorded using an Agilent UV-vis 8453 spectrophotometer under argon. The absorption spectra of the *in situ* electrochemically generated species were measured using a one-compartment, three-electrode quartz cell with 0.1 M $Bu_4NPF_6$ in $CH_3CN$. The working electrode was a platinum grid with a teflon covered wire to ensure electrolysis occurred only at the platinum gauze. The reference and counter electrode were positioned in the top of the cell. Appropriate potentials were applied (−1.69 V vs. $Fc/Fc^+$) using an Autolab PGSTAT100 potentiostat controlled with GPES 4.9 software. During electrolysis, absorption spectra of the electrochemically generated species were recorded at regular intervals for a period of 230 sec (Figure S4). A spectrum was recorded following reoxidation of the solution to check the chemical reversibility.

**Transient Absorption Spectroscopy:** Flash photolysis measurements were collected using a frequency doubled Q-switched Nd:YAG laser (Quanta-Ray ProSeries, Spectra-Physics) to obtain 532 nm pump light (10 mJ/pulse). Probing by a pulsed XBO 450 W Xenon Arc Lamp (Osram) and spectral signal detection by the iStar CCD camera (Andor Technology) of an LP920-S laser flash photolysis spectrometer setup (Edinburgh Instruments) were performed at a right angle with respect to the pump light. Transient signal detection was done with LP920-K PMT detector which was connected to a Tektronix TDS 3052 500 MHz 5 GS/s oscilloscope. Transient absorption spectra were acquired using the L900 software (Edinburgh Instruments) and processed using Origin 9 software. A fluorescence quartz cell cuvette (Starna; Atascadero, CA) with a 10 mm pathlength was used for measurements.

**Photocatalytic $H_2$ Production:** For a typical photocatalytic experiment, each sample was prepared in a 88 mL two-neck round bottom flask containing 10 mL of 1.0 M acetate buffer (pH 4.0), 0.5 mM $[Ru(bpy)_3]Cl_2 \cdot 6H_2O$, and 0.1 M ascorbic acid. The solution was sealed with a septum, degassed for 30 min using argon, and 0.5 ml of pure $H_2$ was injected to activate the $H_2$ sensor before irradiation. Once the amount of $H_2$ reaches constant level (ca. 20 min), 5 µl of a 10 mM stock solution of $[Co(bpma)(H_2O)_2]^{2+}$ catalyst was added using a Hamilton syringe for a final concentration of 5 µM. The samples were irradiated by a 470 nm LED light source at RT with constant stirring. The amount of $H_2$ in the flask's head space (given as a percent) was determined by a HY-OPTIMA Model 740 $H_2$ sensor. The percent $H_2$ was converted to mL using a calibration curve generated by injecting known quantities of $H_2$ in an empty cell.

**Crystallographic Structure Determination:** Single crystals of $[Co(bpma)Cl_2]$ suitable for X-ray diffraction were grown by diffusion of diethyl ether into a methanol solution of the compound at 4°C. X-ray crystallographic data were collected using graphite-monochromatized Mo Kα radiation at 100(1) K on a Bruker Smart APEXII. Data integration and absorption correction were carried out with SAINT (Bruker, Bruker AXS Inc., Madison, Wisconsin USA, 2007) and SADABS (Bruker, Bruker AXS Inc., Madison, Wisconsin USA, 2001), respectively. Structures were solved by direct methods (SHELXS-97) and refined by full-matrix least-squares techniques against $F^2$ (SHELXL-97)[3] using WinGX[4]. Graphical representations are prepared with ORTEP for Windows[5] and POV-Ray. Non-hydrogen atoms were refined using anisotropic displacement parameters.

**EPR Spectroscopy:** The electron paramagnetic resonance (EPR) measurements were performed on a Bruker E500-ELEXSYS spectrometer with an ER DM9807 resonator equipped with an ESR900 cryostat and an Oxford ITC503 temperature controller.

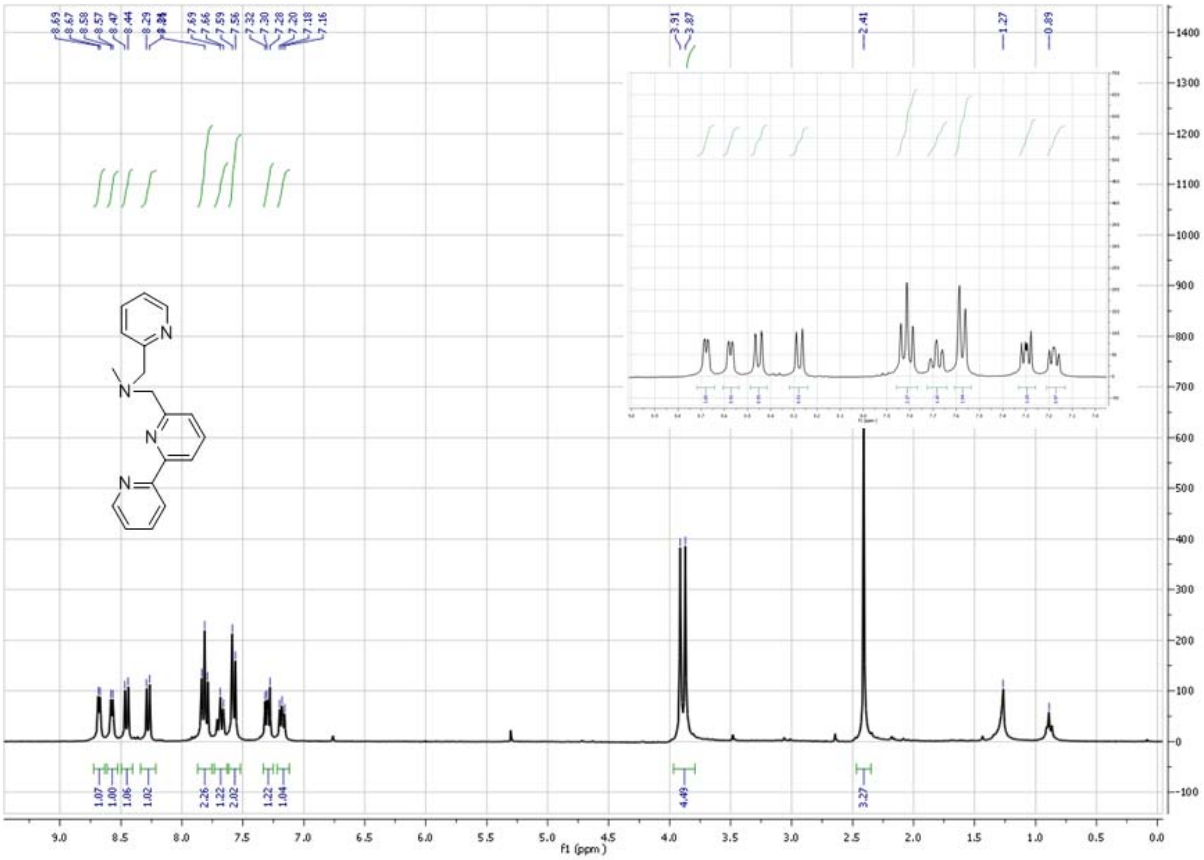


**Figure S1:** $^{1}$H-NMR spectrum ($CDCl_3$, 300 MHz) of bpma ligand at 25°C.

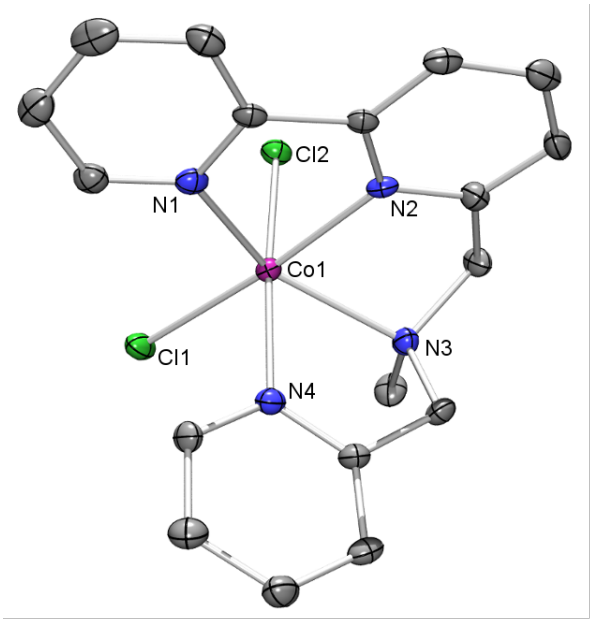


**Figure S2:** Crystal structure of $[Co(bpma)Cl_2]\cdot CH_3OH$ (ORTEP 50% thermal ellipsoid). Hydrogen atoms and methanol molecule of crystallization were omitted for clarity. Bond lengths (Å): Co1-N1 2.155(5), Co1-N2 2.113(4), Co1-N3 2.212(5), Co1-N4 2.169(5), Co1-Cl1 2.4073(15), Co1-Cl2 2.4136(14); Bond angles (°): N2-Co1-N1 74.34(18), N2-Co1-N4 98.14(17), N1-Co1-N4 91.23(18), N2-Co1-N3 74.59(17), N1-Co1-N3 144.71(18), N4-Co1-N3 77.04(18), N2-Co1-Cl1 175.07(13), N1-Co1-Cl1 103.51(13), N4-Co1-Cl1 86.29(12), N3-Co1-Cl1 108.69(13), N2-Co1-Cl2 85.99(13), N1-Co1-Cl2 98.49(12), N4-Co1-Cl2 170.16(14), N3-Co1-Cl2 95.61(13), Cl1-Co1-Cl2 89.97(5).

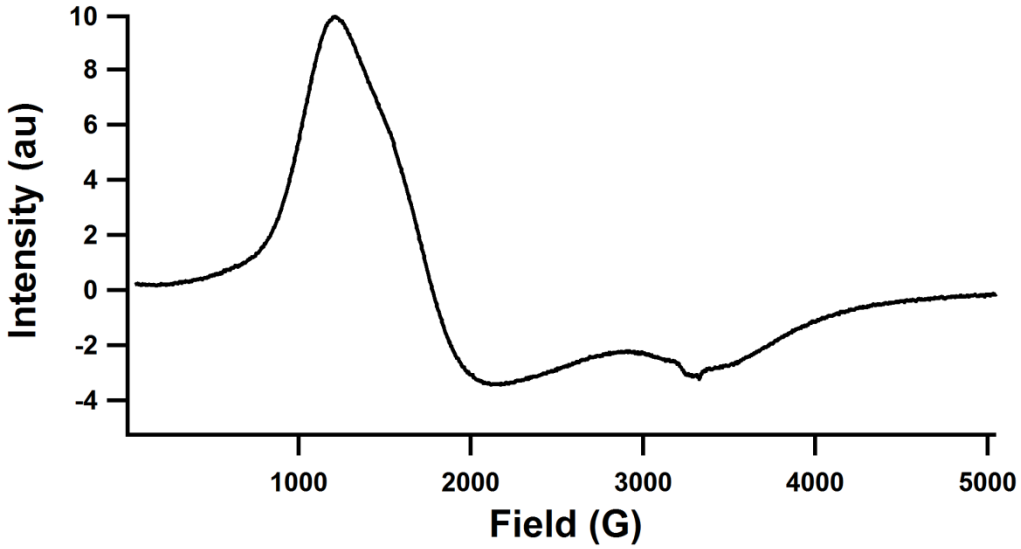


**Figure S3:** EPR spectrum of $[Co(bpma)(H_2O)_2]^{2+}$ measured in $H_2O$ at 9 K using a microwave frequency of 9.3615 GHz and microwave power of 0.2 mW.

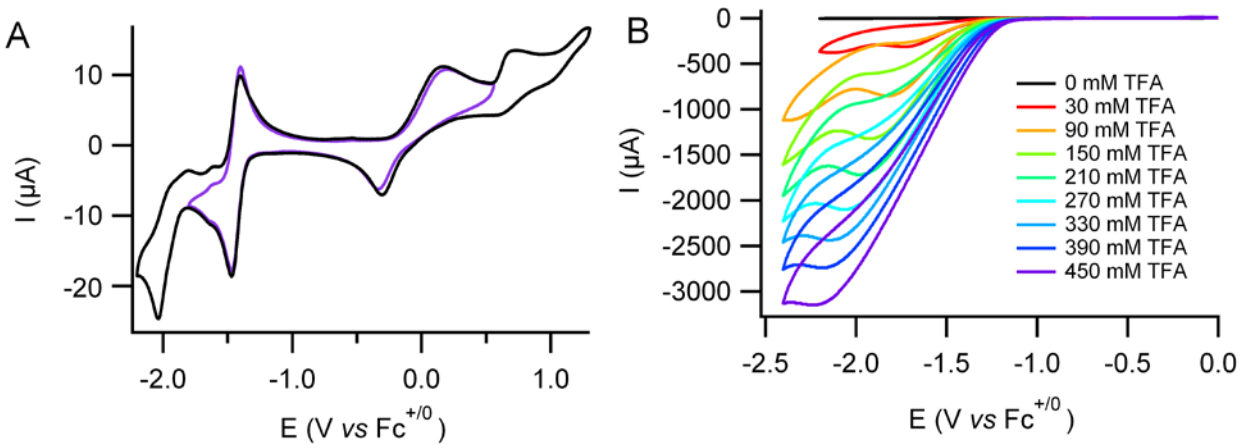


**Figure S4:** (A) Cyclic voltammogram of 1 mM [Co(bpma)$Cl_2$] in $CH_3CN$ using 0.1 M $Bu_4NPF_6$ under an argon atmosphere with a scan rate of 100 mV/s. (B) Cyclic voltammogram of 50 μM [Co(bpma)$Cl_2$] in $CH_3CN$ using 0.1 M $Bu_4NPF_6$ upon the addition of increasing concentrations of trifluoroacetic acid (TFA) at a scan rate of 100 mV/s.

**Table S1:** Electrochemical properties of [Co(bpma)$Cl_2$] in $CH_3CN$ [a]

| Assignment | $E_{½}$ (V) | $\Delta E_p$ (V) | Reversibility |
|---|---|---|---|
| $bpma^{0/+}$ | +0.704 [b] | -- | irreversible |
| $Co^{III/II}$ | −0.08 [c] | 0.434 | quasi-reversible |
| $Co^{II/I}$ | −1.44 | 0.062 | reversible |
| $Co^{I/0}$ | −2.04 [b] | -- | irreversible |

[a] Potentials reported vs. $Fc^{+/0}$. Measured in deoxygenated, argon-saturated, 0.1 M $Bu_4NPF_6$ solutions of $CH_3CN$. [b] $E_p$ [c] of an irreversible process. [c] $E_{½}$ of a quasi-reversible process.

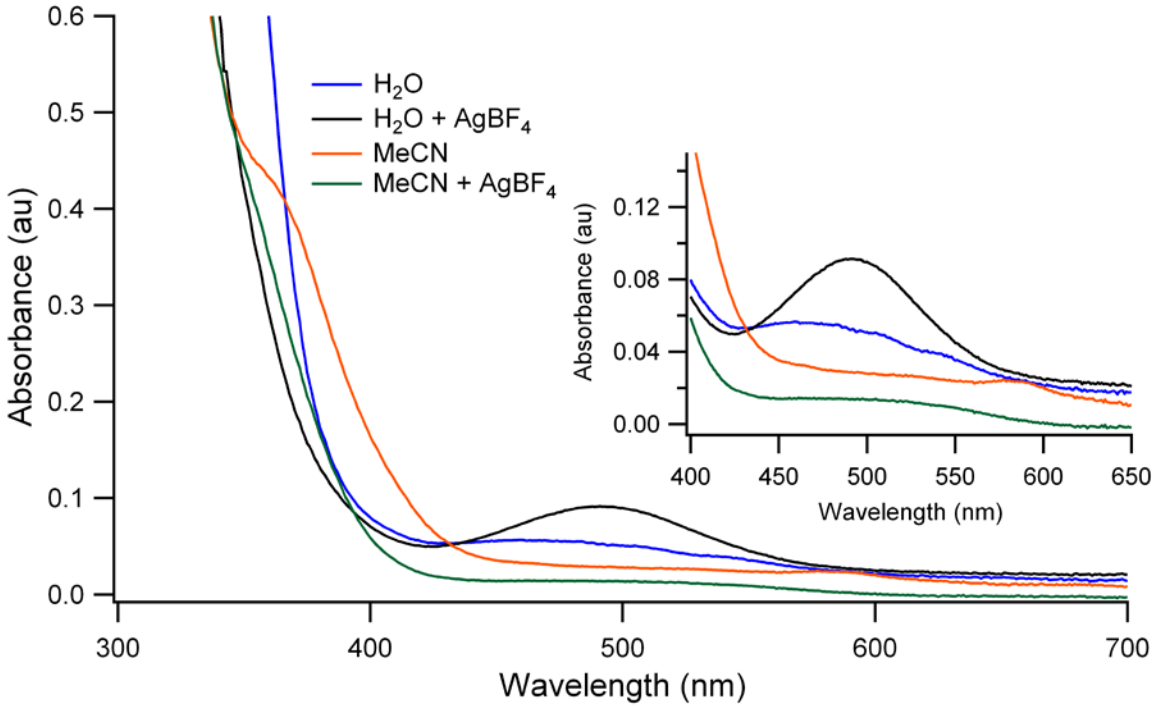


**Figure S5:** Electronic absorption spectra of $[Co(bpma)Cl_2]$ in $CH_3CN$ in the absence (orange line) and presence (green line) of $AgBF_4$. Electronic absorption spectra of $[Co(bpma)(H_2O)_2]^{2+}$ in $H_2O$ in the absence (blue line) and presence (black line) of $AgBF_4$.

**Comment regarding electronic absorption spectra:** The electronic absorption spectra for the title $[Co(bpma)Cl_2]$ complex were measured in $CH_3CN$ in the absence and presence of $AgBF_4$. The visible region displays minimal absorption contributing from the expected $[Co(bpma)Cl_2]$ and $[Co(bpma)(NCCH_3]^{2+}$ complexes in the absence and presence of $Ag^+$, respectively. Conversely, when $[Co(bpma)Cl_2]$ is dissolved in $H_2O$, a broad transition between 450 and 550 nm appears and in the presence of $Ag^+$, the intensity of this transition increases. This Co-based, ligand field transition is strongly influenced by the presence of $Cl^-$, $CH_3CN$, or $H_2O$ ligands. When the complex is dissolved in $H_2O$, the broad transition in the visible region is observed and corresponds to the $[Co(bpma)(H_2O)_2]^{2+}$ complex.

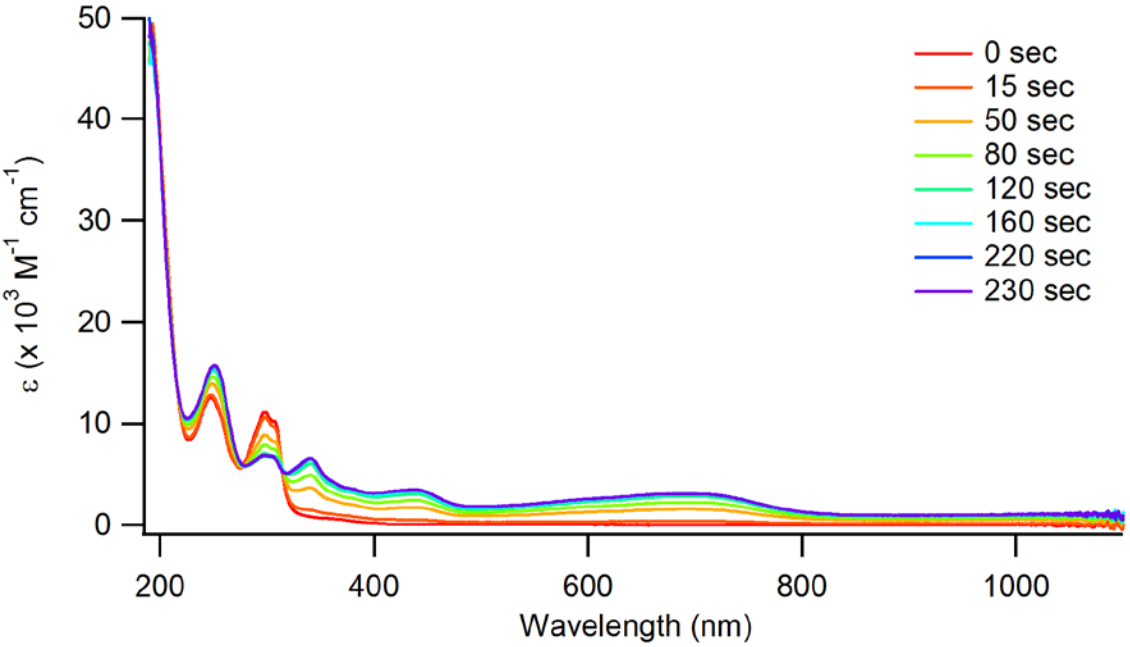


**Figure S6:** Electronic absorption spectra of the one-electron, electrochemically reduced Co(I) species in $CH_3CN$ using 0.1 M $Bu_4NPF_6$. Spectra were collected periodically upon constant potential electrolysis (CPE) with an applied potential of −1.69 V vs. $Fc/Fc^+$.

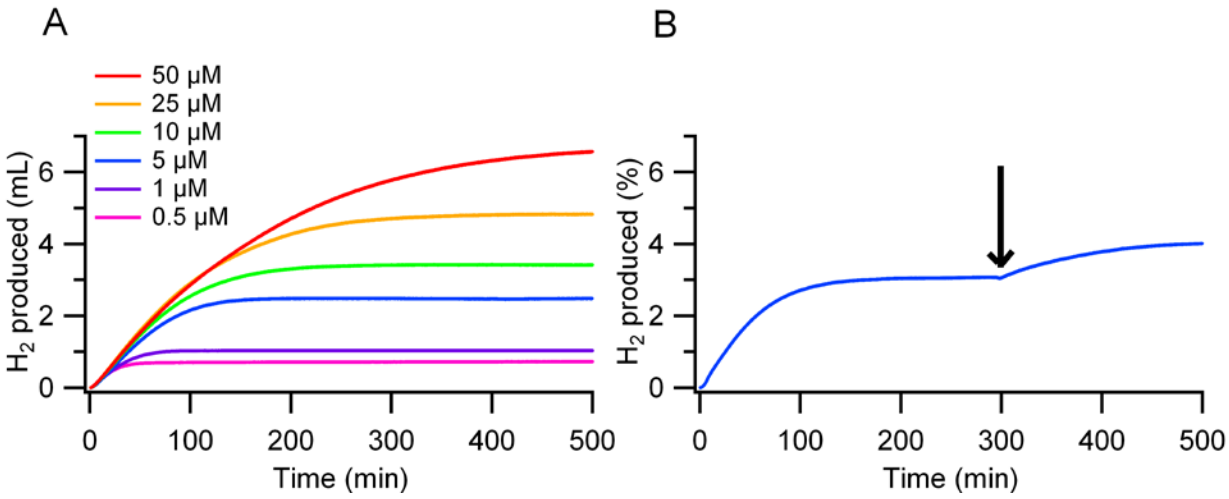


**Figure S7:** (A) Photocatalytic $H_2$ evolution with varying $[Co(bpma)(H_2O)_2]^{2+}$ concentrations in a pH 4 acetate buffer solution containing 0.5 mM $[Ru(bpy)_3]^{2+}$ and 0.1 M ascorbic acid in a 88 mL round bottom flask that was photolysed at 470 nm. (B) Photocatalytic $H_2$ experiment using 5 µM $[Co(bpma)(H_2O)_2]^{2+}$ with the addition of 5 µM of new catalyst solution after 5 h as indicated by the arrow.

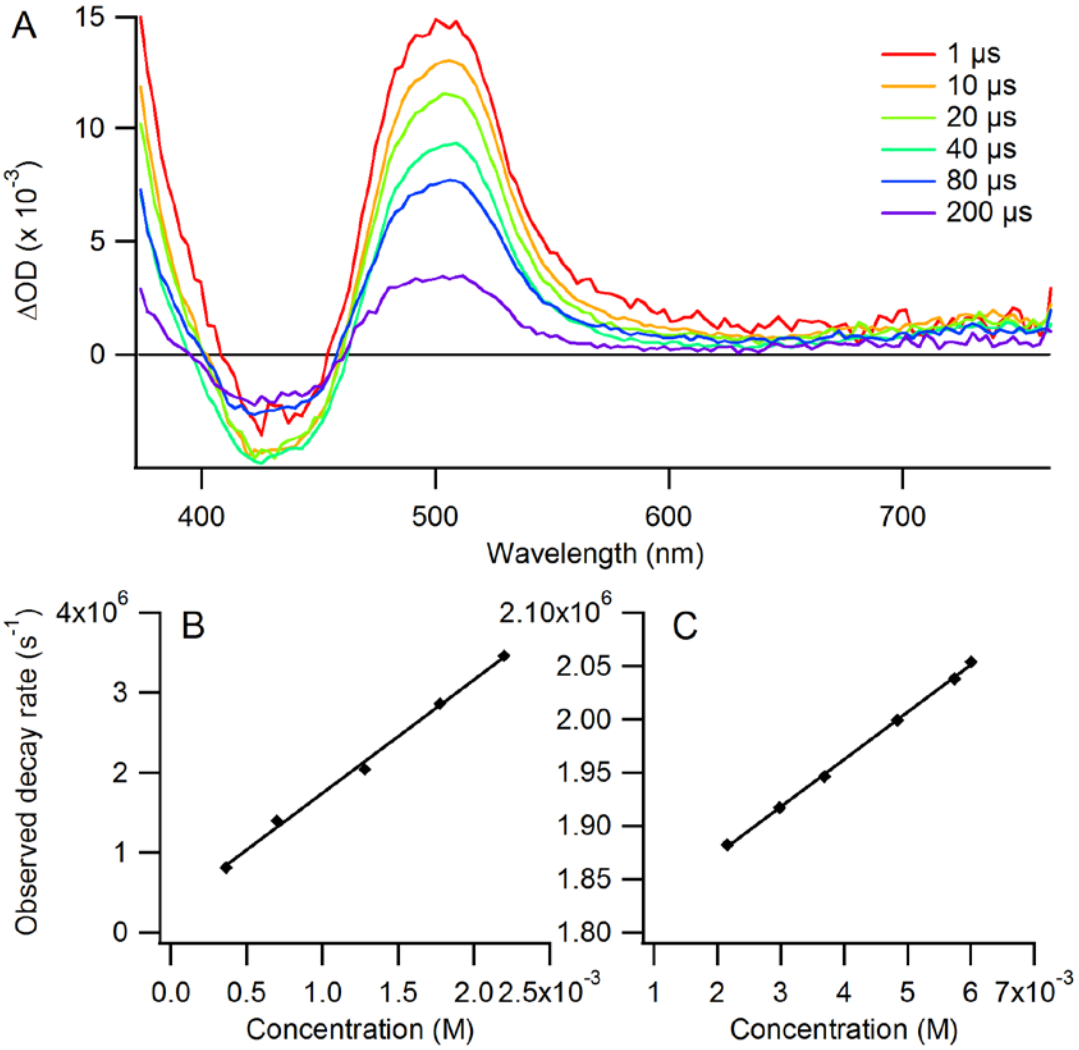


**Figure S8:** (A) Differential absorption spectra of 50 μM $[Ru(bpy)_3]^{2+}$ upon photoexcitation at 532 nm in the presence of 0.1 M ascorbate electron donor in a saturated aqueous sodium bicarbonate solution (pH 8.3). (B) The pseudo-first order decay rate constant for laser flash-generated $[Ru(bpy)_3]^{+}$ from transient absorption at 520 nm as a function of $[Co(bpma)(H_2O)_2]^{2+}$ concentration, giving the second-order rate constant for bimolecular electron transfer ($k_{q2}$). (C) Stern-Volmer analysis of the decay rate constant for laser flash-generated $[Ru(bpy)_3]^{2+*}$ emission at 630 nm as a function of $[Co(bpma)(H_2O)_2]^{2+}$ concentration in the absence of ascorbate electron donor, suggestion excited state quenching by exchange energy transfer to the Co complex.

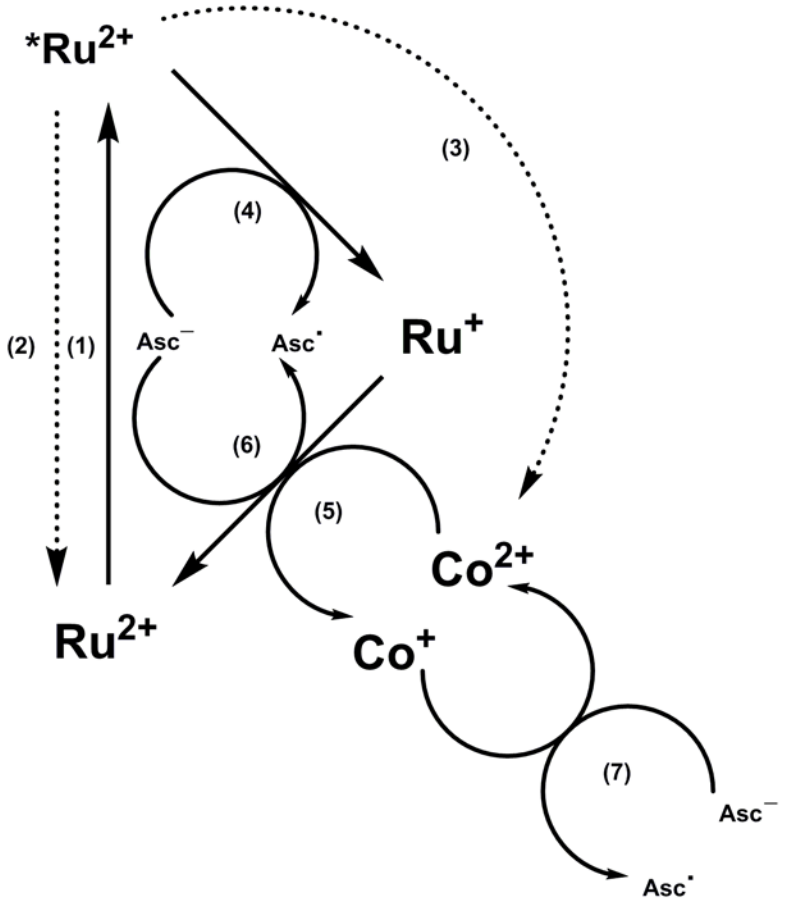


| | | |
|---|---|---|
| Photoexcitation: $Ru^{2+} \xrightarrow{h\nu} {}^*Ru^{2+}$ | | (1) |
| Excited state relaxation: $^*Ru^{2+} \longrightarrow Ru^{2+}$ | $1.8*10^6\ s^{-1}$ | (2) |
| Energy transfer: $^*Ru^{2+} + Co^{2+} \longrightarrow Ru^{2+} + Co^{2+}$ | $4.4*10^7\ M^{-1}\ s^{-1}$ | (3) |
| Reductive quenching: $^*Ru^{2+} + Asc^- \longrightarrow Ru^+ + Asc^·$ | $4*10^7\ M^{-1}\ s^{-1}$ | (4) |
| Electron transfer: $Ru^+ + Co^{2+} \longrightarrow Ru^{2+} + Co^+$ | $1.4*10^9\ M^{-1}\ s^{-1}$ | (5) |
| Recombination: $Ru^+ + Asc^· \longrightarrow Ru^{2+} + Asc^-$ | $2*10^{10}\ M^{-1}\ s^{-1}$ | (6) |
| Recombination: $Co^+ + Asc^· \longrightarrow Co^{2+} + Asc^-$ | $8*10^9\ M^{-1}\ s^{-1}$ | (7) |

**Scheme S1.** Scheme depicting the initial steps within the photocatalytic process following photoexcitation of $[Ru(bpy)_3]^{2+}$. $Ru^{2+}$ = $[Ru(bpy)_3]^{2+}$ photosensitizer; $Co^{2+}$ = $[Co(bpma)(H_2O)_2]^{2+}$ catalyst; $Asc^-$ = ascorbate electron donor.

**Reduced catalyst deactivation processes**: Following reduction of $[Co(bpma)(H_2O)_2]^{2+}$ by $[Ru(bpy)_3]^+$, multiple deactivation pathways for $[Co(bpma)(H_2O)_2]^+$ are available. The $Co^I$ species can enter the catalytic cycle through protonation to generate a $Co^{III}$-hydride and eventually evolve $H_2$ gas, while regenerating the $Co^{II}$ initial species. The potential deactivation pathways also include recombination of the $Co^{III}$-hydride or the $Co^I$ species with the ascorbate radical. While all processes are possible, only one

process appears to dominate the observed decay following $Co^{I}$ formation. The quantum yield for hydrogen production at high pH appears to be low, indicating that recombination rather than regeneration is the main process. The decay at 700 nm is second-order in nature, indicating that it is not a protonation step occurring as a pseudo-first order decay would appear. The same conclusion can be made by noting that the signal at 700 nm returns to zero, therefore going back to the ground state and not to a $Co^{III}$-hydride species since this would have spectral features distinct from $Co^{II}$ and $Co^{I}$. Recombination between the $Co^{I}$ species and the ascorbate radical are determined to be the dominating pathway for deactivation of $Co^{II}$ which explains the decay of the signal at 700 nm.

**Table S2:** Crystallographic data and structure refinement of $[Co(bpma)Cl_2]$.

| | |
|---|---|
| Compound name | $[Co(bpma)Cl_2]$ |
| Empirical formula | $C_{19}H_{22}Cl_2CoN_4O$ |
| Formula weight | 452.24 |
| Crystal system | monoclinic |
| Space group | P 21/n |
| a /Å | 8.3723(9) |
| b /Å | 15.8181(16) |
| c /Å | 15.0692(16) |
| α/° | 90.00 |
| β/° | 104.561(7) |
| γ/° | 90.00 |
| Volume/$Å^3$ | 1931.6(4) |
| Z | 4 |
| $\rho_{calc}mg/mm^3$ | 1.555 |
| $m/mm^{-1}$ | 1.182 |
| F(000) | 932 |
| 2θ range for data collection | 1.90 to 26.42° |
| Index ranges | $-10 \leq h \leq 9$, $-19 \leq k \leq 19$, $-18 \leq l \leq 14$ |
| Total reflections collected | 14727 |
| Completeness to 2θ/% | 99.6 |
| Data/restraints/parameters | 3958/0/246 |
| Goodness of fit on $F^2$ | 1.131 |
| Final R indices [$I > 2\sigma(I)$] | $R_1 = 0.0573$, $wR_2 = 0.1587$ |
| Final R indices (all data) | $R_1 = 0.0984$, $wR_2 = 0.2394$ |
| Largest diff. peak/hole /e $Å^{-3}$ | 0.976/-1.899 |

## References

1. T. Murashima, S. Tsukiyama, S. Fujii, K. Hayata, H. Sakai, T. Miyazawa and T. Yamada, *Org. Biomol. Chem.*, 2005, **3**, 4060-4064.
2. H. T. S. Britton and R. A. Robinson, *Journal of the Chemical Society (Resumed)*, 1931, 1456-1462.
3. G. M. Sheldrick, *Acta Crystallographica Section A*, 2008, **64**, 112-122.
4. L. Farrugia, *Journal of Applied Crystallography*, 1999, **32**, 837-838.
5. L. Farrugia, *Journal of Applied Crystallography*, 1997, **30**, 565.